ELSEVIER

PII: S0032-3861(96)01000-2

Polymer Vol. 38 No. 10, pp. 2389–2397, 1997

0032-3861/97/$17.00 + 0.00

Vibrational dynamics and heat capacity of β-poly(L-serine)

Archana Gupta, Poonam Tandon, Vishwambhar Dayal Gupta* and Shantanu Rastogi

Physics Department, Lucknow University, Lucknow – 226007, India

(Received 29 January 1996)

Poly(L-serine) is a poly(amino acid) having a side group ($-CH_2OH$). It is found to exist in an anti-parallel β sheet structure. A study of complete normal modes and their dispersion has been carried out using Higg's modification of Wilson's GF matrix method and the Urey–Bradley force field. The constants of the field have been best fitted to the Fourier transform infra-red and Raman frequencies. Repulsion and exchange of character between various pairs of modes have been observed. Heat capacity as a function of temperature, obtained from the dispersion curves via density-of-states, is in good agreement with the measurements of Roles *et al.* (*Biopolymers*, 1993, **33**, 753). © 1997 Elsevier Science Ltd.

(Keywords: conformation; anti-parallel β sheet; phonon dispersion)

INTRODUCTION

Poly(L-serine) [PLS] (*Figure 1*) is a high molecular weight peptide and may serve as a model compound in the characterization of various physiological functions of proteins with a high serine content, e.g. silk fibroin and phasvitin[1]. Several studies have been made on the conformation of PLS[1–6]. Initially it was postulated by Fasman and Blout[2] that, in aqueous solution and in the solid state, PLS exists in random conformation. Later X-ray and infra-red (i.r.) studies established that in the solid state PLS has an anti-parallel β structure[1,3,4]. On the basis of energy map calculations, a left-handed α-helical conformation has also been predicted for PLS by Sarathy and Ramachandran[5]. They have argued that the α structure can be further stabilized by the formation of an intramolecular hydrogen bond between the hydroxyl group in the side chain and a carbonyl oxygen of the backbone. However, no experimental evidence has been found for an α helical conformation in PLS[1,3,4].

Infra-red spectroscopy plays an important role in polypeptide characterization, determining crystallinity, conformation, intra- and inter-molecular hydrogen bonding, fold structure of polymers, composition and sequence distribution in copolymers. Normal mode analysis provides a detailed understanding of the vibrational spectrum and force field for a molecule of known structure. Through the dispersion curves, the microscopic behaviour of the crystal can be correlated with its macroscopic properties such as specific heat, internal energy, entropy, etc. In recent publications Wunderlich and co-workers[7–10] have reported experimental and theoretical studies of heat capacities based on vibrational analysis of a variety of polymeric systems, synthetic as well as biopolymeric. In most of the cases, their analysis is based on the separation of the vibrational spectrum into group and skeletal vibrations. The former are taken from computations fitted to i.r. and Raman data, and the latter by using the two-parameter Tarasov model[7] and fitting it to low temperature heat capacities. However, in a few cases, where detailed dispersion curves of the vibrational spectrum are available[11–13], they have been used for obtaining group and skeletal vibrations and the number of vibrators of each type. In some cases, dispersion curves for one polymeric system have been used to obtain the number of vibrators and frequencies of box oscillators for polymers with identical backbone. When full dispersion curves are not available, this approach may be adopted. However, it has its own limitations, specially when the side chain and backbone modes are strongly coupled. Infra-red and Raman spectroscopic studies of PLS (β form) have been reported by Bohak and Ellenbogen[14] and Koenig and Sutton[4]. Their assignments are both incomplete and are based on qualitative considerations. It is, therefore, all the more important to carry out a complete normal mode analysis and their dispersions for PLS. In the present communication we report for PLS a study of complete normal modes and their full dispersions within the first Brillouin zone. Specific heat data obtained from dispersion curves are found to be in better agreement with the experimental measurements.

THEORY AND EXPERIMENT

Calculation of normal mode frequencies

The calculation of normal mode frequencies has been carried out according to Wilson's GF matrix method[15–17] as modified by Higgs[18] for an infinite polymeric chain. In brief, the vibrational secular equation, which gives normal mode frequencies, has the form:

$$[G(\delta)F(\delta) - \lambda(\delta)I] = 0, \qquad 0 \leq \delta \leq \pi \qquad (1)$$

* To whom correspondence should be addressed

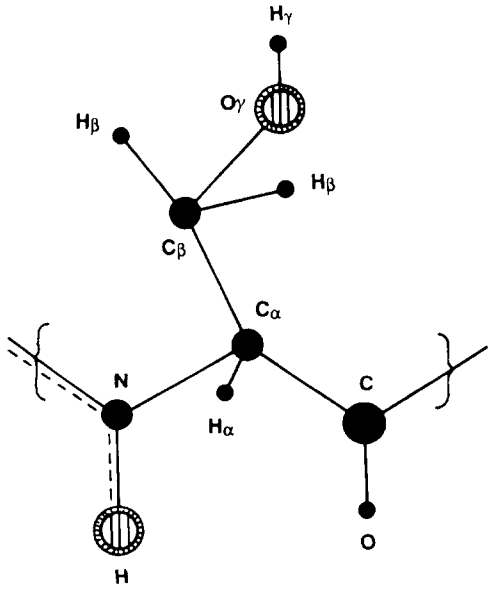

Figure 1 A chemical repeat unit of poly(L-serine)

where G is the inverse of the kinetic energy matrix, F is the force field matrix, and δ is the vibrational phase difference between the corresponding modes of the adjacent residue units.

The vibrational frequencies $\nu(\delta)$ (in cm^{-1}) are related to eigenvalues $\lambda(\delta)$ by the following relation:

$$\lambda_i(\delta) = 4\pi^2 c^2 \nu_i^2(\delta) \tag{2}$$

A plot of $\nu_i(\delta)$ *versus* δ gives the dispersion curve for the ith mode.

Calculation of specific heat

Dispersion curves can be used to calculate the specific heat of a polymeric system. For a one-dimensional system the density of state function or the frequency distribution function, which expresses the way energy is distributed among the various branches of normal modes in the crystal, is calculated from the relation:

$$g(\nu) = \sum_j (\partial \nu_j / \partial \delta)^{-1}|_{\nu_j(\delta)=\nu} \tag{3}$$

The sum is over all branches j. Considering a solid as an assembly of harmonic oscillators, the frequency distribution $g(\nu)$ is equivalent to a partition function.

The heat capacity can give information about the proportion of various conformational states present in the material. For example, in the case of a protein it can give information about the proportion which is in α helical or β sheet structure. This is necessary in evaluating the basic thermodynamics of enzyme reactions. The constant volume heat capacity can be calculated using Debye's relation:

$$C_v = \sum_j g(\nu_j) k N_A (h\nu_j/kT)^2 \frac{\exp(h\nu_j/kT)}{[\exp(h\nu_j/kT) - 1]^2} \tag{4}$$

with

$$\int g(\nu_i)\, d\nu_i = 1 \tag{5}$$

The constant volume heat capacity C_v, given by equation (4) is converted into constant pressure heat capacity C_p using the Nernst–Lindemann approximation[9]:

$$C_p - C_v = 3RA_0(C_p^2 T / C_v T_m^0) \tag{6}$$

where A_0 is a constant often of a universal value $[3.9 \times 10^{-9}\ (K\,mol)\,J^{-1}]$ and T_m^0 is the estimated equilibrium melting temperature, which is taken to be 573 K.

The Fourier transform i.r. (*FT*i.r.) spectra of PLS purchased from Sigma Chemicals (P-5887 lot no. 91H5511) has been recorded on a Perkin Elmer 1800 spectrometer. The sample was prepared by mixing PLS in CsI and pressing into the form of a pellet. Before recording the spectra, the equipment was purged with dry nitrogen. The observed spectra are depicted in *Figure 2*.

RESULTS AND DISCUSSION

On the basis of the energy minimization technique, Chou *et al.*[6] have shown that a parallel β sheet is more stable for PLS and that it has a negative value of twist. However, experimental evidence points to an anti-parallel β sheet structure for PLS. For the present calculations an anti-parallel β structure is assumed. The dihedral angles used for this conformation, as given by Chou *et al.*[6], are $\phi = -155°$, $\psi = 146°$, $\omega = -178°$, $\chi^1 = 62°$ and $\chi^2 = -52°$.

The unit cell of PLS consists of two repeat units. There are 11 atoms per residue unit, which will give rise to 33 dispersion curves. The Urey–Bradley force field has been used for calculations. It gives a better description of the intra-unit interactions and of the interactions due to neighbouring units (*Table 1*). In cases where direct force constants cannot be used for matching, one can feed off-diagonal interactions between internal coordinates. Values of these interactions depend on the geometry of the atoms involved in those internal coordinates. A good fit of calculated frequencies with the observed *FT* i.r. spectra is obtained by adjusting the force field. The assignments have been made on the basis of potential energy distribution, line profile, and line intensity in *FT* i.r. and second derivative spectra.

The dispersion of modes below 1700 cm^{-1} are plotted in *Figures 3a*, *4a* and *5a*. All modes above this are either non-dispersive or their dispersion is within 5 cm^{-1} and hence they are not shown. As shown in *Figure 5a* the two lowest lying branches ($\nu = 0$ at $\delta = 0$ and $\delta = \pi$) are the four acoustic modes. At $\delta = 0$ the two acoustic branches correspond to the translational mode along the chain axis and the rotational mode about the axis. At $\delta = \pi$ they correspond to the translational modes perpendicular to the axis.

For the sake of simplicity the modes are discussed under two separate heads, viz. backbone modes and side chain modes. Pure backbone modes are given in *Table 2* and pure side chain modes in *Table 3*. The modes involving the coupling backbone and side chain are given in *Table 4*.

Backbone modes

Modes involving the motions of main chain atoms (–C–Cα–N–) are termed as backbone modes.

Amide groups of polypeptides are strong chromophores in i.r. absorption, and these groups give rise to strong characteristic bands (amide A, I–VII). These amide modes along with other characteristic modes have been used for structural diagnosis. Based on such

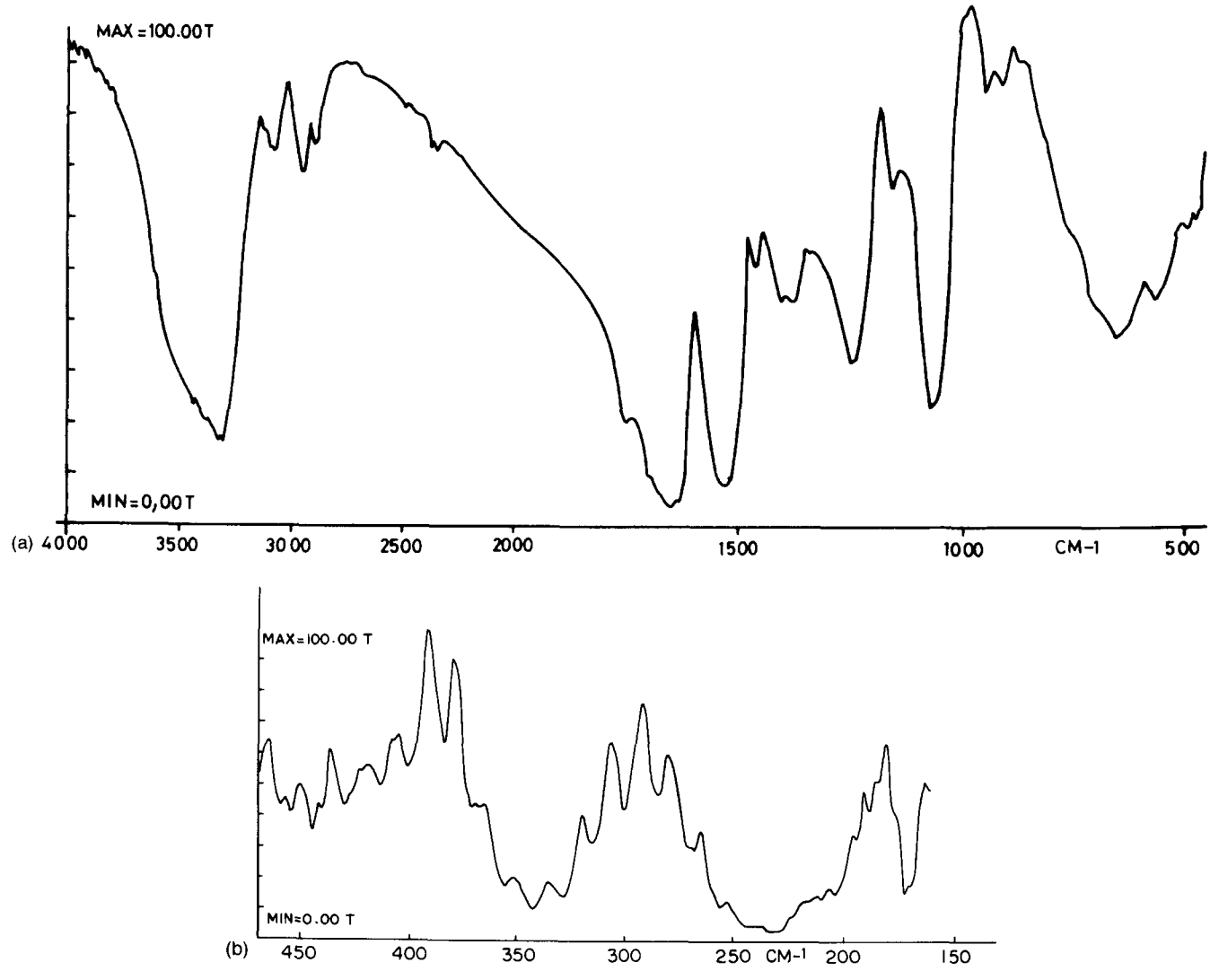

Figure 2 (a) *FT* i.r. spectra of PLS (4000–450 cm^{-1}); (b) *FT* i.r. spectra of PLS (450–150 cm^{-1})

Table 1 Internal coordinates and force constants (md $Å^{-1}$)

$\nu(O_\gamma-H_\gamma)$	6.2500	ϕ(H–N=C)	0.370 (.60)
ν(N–H)	5.4800	$\phi(H-N-C_\alpha)$	0.350 (.47)
$\nu(C_\alpha-H_\alpha)$	4.1460	$\phi(H_\alpha-C_\alpha-N)$	0.220 (.80)
$\nu(C_\beta-H_\beta)$	4.2330	ϕ(O=C=N)	0.520 (1.3)
$\nu(C_\alpha-C)$	2.1500	$\phi(O=C-C_\alpha)$	0.360 (.60)
$\nu(C_\alpha-C_\beta)$	3.3000	$\phi(O_\gamma-C_\beta-C_\alpha)$	0.510 (.30)
$\nu(N-C_\alpha)$	3.3000	$\phi(O_\gamma-C_\beta-H_\beta)$	0.300 (.34)
ν(N=C)	5.3500	$\phi(H_\gamma-O_\gamma-C_\beta)$	0.565 (.50)
ν(C=O)	8.3100	$\phi(H_\beta-C_\beta-C_\alpha)$	0.480 (.22)
$\nu(C_\beta-O_\gamma)$	4.3200	$\phi(H_\alpha-C_\alpha-C)$	0.300 (.48)
ω(C=O)	0.3400	$\phi(C-C_\alpha-C_\beta)$	0.430 (.20)
ω(N–H)	0.1340	$\phi(N-C_\alpha-C_\beta)$	0.220 (.48)
$\omega(O_\gamma-H_\gamma)$	0.0790	$\phi(N-C-C_\alpha)$	0.210 (.60)
$\tau(C_\alpha-C)$	0.0900	$\phi(H_\alpha-C_\alpha-C_\beta)$	0.370 (.20)
τ(C=N)	0.0350	$\phi(C=N-C_\alpha)$	0.650 (.35)
$\tau(N-C_\alpha)$	0.0550	$\phi(N-C_\alpha-C)$	0.220 (.48)
$\tau(C_\alpha-C_\beta)$	0.0250	$\phi(H_\beta-C_\beta-H_\beta)$	0.410 (.25)
$\tau(C_\beta-O_\gamma)$	0.0065		
	Off-diagonal interactions		
	$\nu(N-C_\alpha)-\nu$(N=C)	.25	
	$\nu(C_\alpha-C)-\nu$(N=C)	.15	
	$\nu(C_\alpha-C)-\phi(C_\alpha-C_\beta-H_\beta)$	.05	

Note: ν, ϕ, ω and τ denote stretch, angle bend, wag and torsion, respectively
Non-bonded force constants are given in parentheses

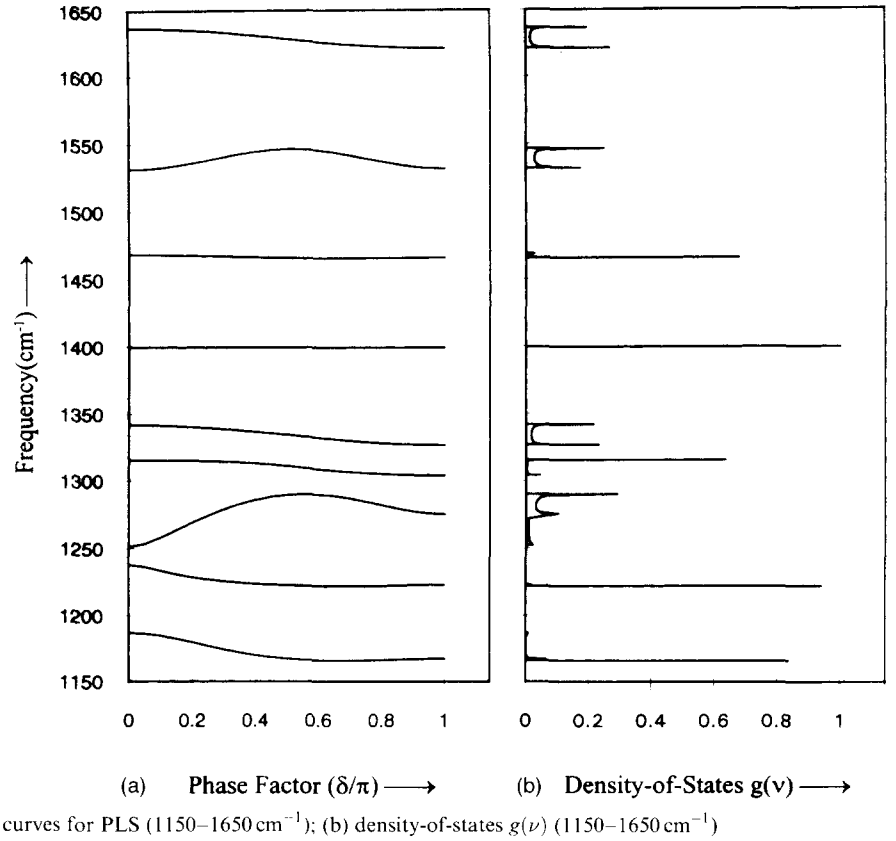

Figure 3 (a) Dispersion curves for PLS (1150–1650 cm^{-1}); (b) density-of-states $g(\nu)$ (1150–1650 cm^{-1})

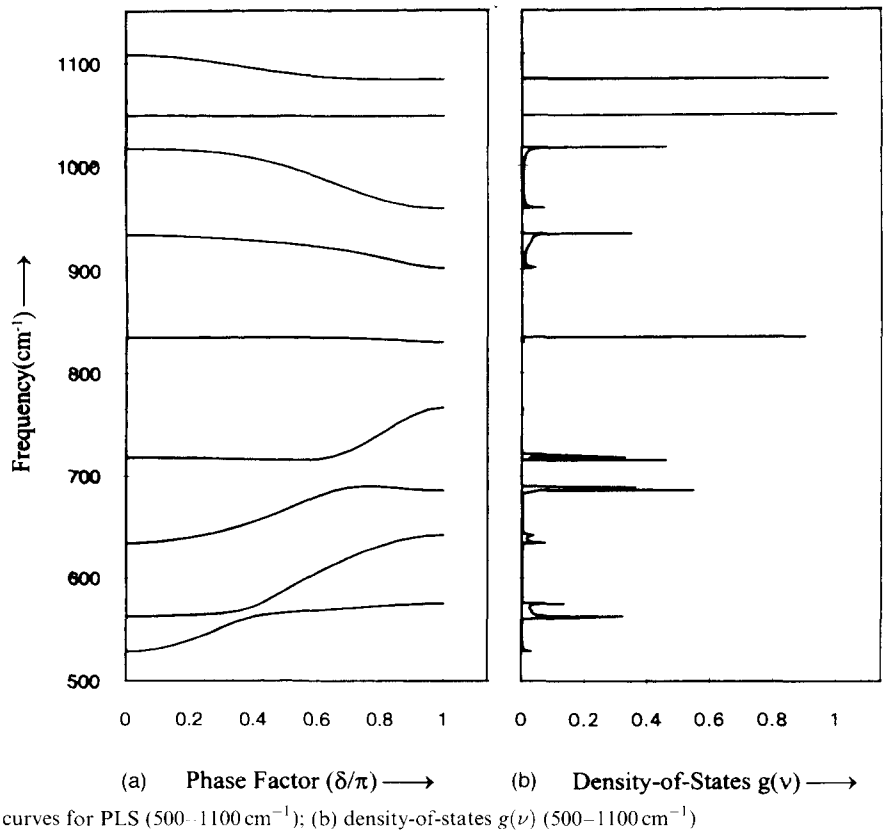

Figure 4 (a) Dispersion curves for PLS (500–1100 cm^{-1}); (b) density-of-states $g(\nu)$ (500–1100 cm^{-1})

diagnostic correlations, attempts have been made to estimate secondary structural composition in proteins.

The amide A band, which arises due to the N–H stretch, is not too sensitive to the chain conformation and side-chain structure, but is highly sensitive to the strength of the N–H...O=C hydrogen bond. As seen from *Table 3*, amide A in PLS has a frequency which is higher than in other β sheets. This is attributed to a weaker hydrogen bond in PLS. One of the factors contributing to the weakness of the hydrogen bond could

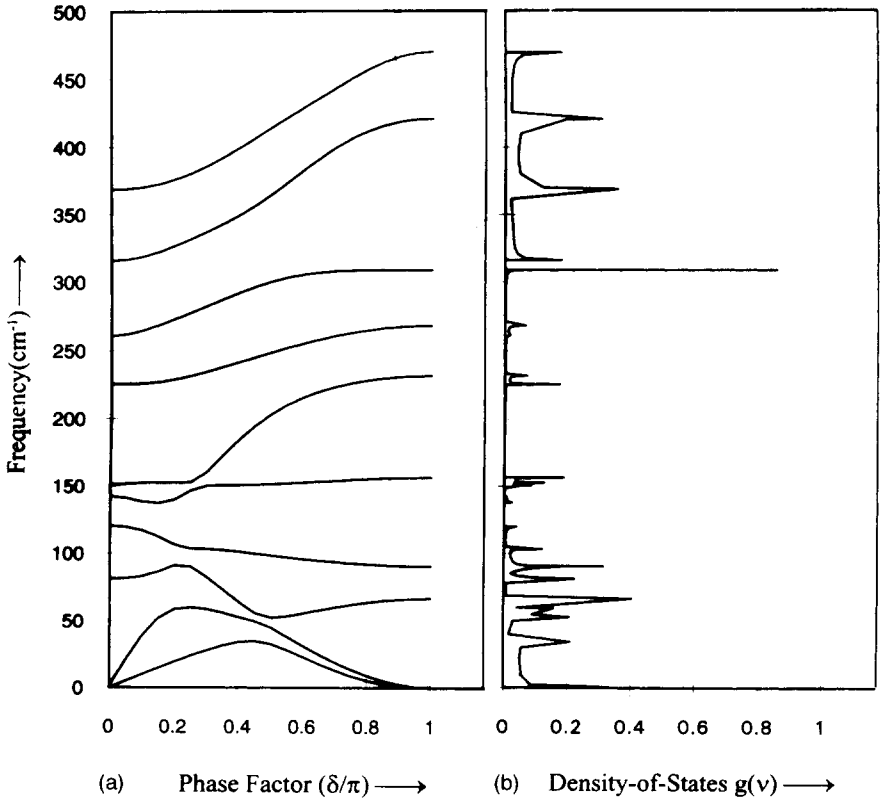

Figure 5 (a) Dispersion curves for PLS (below 500 cm^{-1}); (b) density-of-states $g(\nu)$ (below 500 cm^{-1})

Table 2 Pure backbone models

Calc.	Obs.	Assignment (% PED at $\delta = 0.0$)	Calc.	Obs.	Assignment (% PED at $\delta = \pi$)
3318	3318	ν(N–H)(100) (Amide A)	3318	3318	ν(N–H)(100) (Amide A)
1637	1628	ν(C=O)(66) + ν(N=C(18) (Amide I)	1621	1628	ν(C=O(66) + ν(N=C)(13) (Amide I)
1532	1537	ν(N=C)(18) + ϕ(H–N–C_α)(36) + ϕ(H–N=C)(36) (Amide II)	1532	1528	ϕ(H–N–C_α) + ν(N=C)(26) + ϕ(H–N=C)(29) (Amide II)

Table 3 Pure side-chain modes

Calc.	Obs.	Assignment (% PED at $\delta = 0.0$)
3384	3382	$\nu(O_\gamma–H_\gamma)(100)$
2967	2963	$\nu(C_\alpha–H_\alpha)(99)$
2925	2930	$\nu(C_\beta–H_\beta)(99)$
2894	2888	$\nu(C_\beta–H_\beta)(100)$
1469	1467	$\phi(H_\beta–C_\beta–H_\beta)(57) + \phi(H_\gamma–O_\gamma–C_\beta)(16) + \phi(H_\beta–C_\beta–C_\alpha)(16)$
1400	1404	$\phi(H_\gamma–O_\gamma–C_\beta)(76) + \phi(H_\beta–C_\beta–H_\beta)(14)$
1050	1049	$\nu(C_\beta–O_\gamma)(72) + \phi(O_\gamma–C_\beta–H_\beta)(14) + \phi(H_\beta–C_\beta–C_\alpha)(5)$

All frequencies are in cm^{-1}
Only dominant PEDs are given

be involvement of carbonyl oxygen (which binds itself to N–H) in a bifurcated hydrogen bond. As evident from the interatomic distances, there is no intra-chain hydrogen bonding between side-chain hydroxyl and backbone C=O. The distance between the O of the hydroxyl of the side chain and the O of the carbonyl group in the backbone is 4.81 Å. With this distance there is little possibility of intrachain hydrogen bonding between the two oxygens. However, this does not preclude the possibility of an interchain hydrogen bond being formed between the oxygen of the carbonyl group in the main chain and the hydroxyl of the side group in the neighbouring chain. This would imply the possibility of a bifurcated hydrogen bond, which should be reflected in the corresponding band position and profile. In fact, it does appear to be so. The amide I position in PLS appears at 1637 cm^{-1} ($\delta = 0$) and 1628 cm^{-1} ($\delta = \pi$). Apart from this there is an absorption band at a higher value (1678 cm^{-1}). We are finding it difficult to assign this band to any normal mode. However, if one assumes, on a statistical basis, the simultaneous presence of carbonyl groups which are involved in single as well as bifurcated hydrogen bonds, then the 1678 cm^{-1} mode, which is both broad and asymmetric, can be assigned to a carbonyl stretch wherein oxygen is involved in bifurcated hydrogen bonds. All this is based on the existence of a bifurcated hydrogen bond, which must await confirmation from molecular modelling. The complicating factor lies in the size of the side chain because it would affect both the chain packing and the consequential hydrogen bond strength.

Amide II has been calculated at 1533 cm^{-1} corresponding to the observed peak at 1537 cm^{-1}. It disperses and reaches 1527 cm^{-1} and has been matched to 1528 cm^{-1} at $\delta = \pi$. These assignments agree well with those reported by Bohak and Katchalski[1] (1530 cm^{-1})

Table 4 Mixed modes

Calc.	Obs.	Assignment (% PED at $\delta = 0.0$)	Calc.	Obs.	Assignment (% PED at $\delta = \pi$)
1342	1338	$\phi(O_\gamma-C_\beta-H_\beta)(20) + \nu(C_\beta-O_\gamma)(17) + \nu(C_\alpha-C_\beta)(16) + \phi(H_\beta-C_\beta-C_\alpha)(15)$	1326	1338	$\nu(C_\alpha-C_\beta)(19) + \phi(O_\gamma-C_\beta-H_\beta)(16) + \upsilon(C_\beta-O_\gamma)(14) + \phi(H_\beta-C_\beta-C_\alpha)(14)$
1315	1315	$\phi(H_\alpha-C_\alpha-N)(56) + \phi(H_\alpha-C_\alpha-C)(12) + \phi(H_\alpha-C_\alpha-C_\beta)(8)$	1304	1304	$\phi(H_\alpha-C_\alpha-N)(59) + \phi(H_\alpha-C_\alpha-C)(20)$
1251	1249 1275	$\nu(N=C)(33) + \nu(C=O)(10) + \nu(C_\alpha-C)(9) + \phi(H-N-C_\alpha)(7) + \phi(O=C=N)(7) + \nu(N-C_\alpha)(5) + \phi(H_\alpha-C_\alpha-C_\beta)(6) + \phi(H_\alpha-C_\alpha-C)(6) + \phi(H-N=C)(5)$ (Amide III)	1270		$\nu(N=C)(17) + \nu(C_\beta-O_\gamma)(10) + \nu(C_\alpha-C)(11) + \phi(O_\gamma-C_\beta-H_\beta)(10) + \nu(C=O)(9) + \phi(H_\beta-C_\beta-C_\alpha)(14) + \nu(N-C_\alpha)(8)$
1238	1239	$\phi(H_\alpha-C_\alpha-C)(29) + \nu(N-C_\alpha)(16) + \phi(H_\alpha-C_\alpha-C_\beta)(14) + \phi(H_\beta-C_\beta-C_\alpha)(11)$	1223	1216	$\phi(H_\alpha-C_\alpha-C)(30) + \phi(H_\alpha-C_\alpha-C_\beta)(24) + \nu(C_\alpha-C)(10)$
1187	1175	$\phi(H_\beta-C_\beta-C_\alpha)(23) + \nu(N-C_\alpha)(19) + \nu(C_\alpha-C)(11) + \phi(O_\gamma-C_\beta-H_\beta)(10)$	1167	1159	$\phi(H_\beta-C_\beta-C_\alpha)(46) + \phi(O_\gamma-C_\beta-H_\beta)(19) + \nu(N-C_\alpha)(16)$
1108	1117	$\phi(H_\beta-C_\beta-C_\alpha)(31) + \phi(O_\gamma-C_\beta-H_\beta)(23) + \nu(N-C_\alpha)(18)$	1083	1077	$\nu(N-C_\alpha)(29) + \nu(C_\alpha-C_\beta)(20) + \phi(H_\beta-C_\beta-C_\alpha)(15) + \phi(O_\gamma-C_\beta-H_\beta)(13)$
1017	1025	$\nu(C_\alpha-C)(33) + \nu(C_\alpha-C_\beta)(9) + \phi(C=N-C_\alpha)(9)$	959	948	$\nu(C_\alpha-C_\beta)(35) + \nu(N-C_\alpha)(22) + \phi(O_\gamma-C_\beta-H_\beta)(11)$
934	934	$\nu(C_\alpha-C_\beta)(38) + \phi(O_\gamma-C_\beta-H_\beta)(10) + \nu(N-C_\alpha)(9)$	901	903	$\nu(C_\alpha-C)(44) + \phi(O=C=N)(12)$
835	835	$\phi(O_\gamma-C_\beta-H_\beta)(43) + \phi(H_\beta-C_\beta-C_\alpha)(29)$	830	835	$\phi(O_\gamma-C_\beta-H_\beta)(34) + \phi(H_\beta-C_\beta-C_\alpha)(26)$
718	713	$\omega(N-H)(50 + \omega(C=O)(16)$ (Amide V)	766	773	$\phi(O=C=N)(19) + \phi(C=N-C_\alpha)(15) + \nu(N-C_\alpha)(10)$ (Amide IV)
634	625	$\phi(O=C=N)(16) + \omega(N-H)(12) + \tau(N-C_\alpha)(13) + \tau(C=N)(9) + \phi(O=C-C_\alpha)(7)$	686	685	$\omega(N-H)(68) + \tau(C=N)(11)$ (Amide V)
563	564	$\omega(O_\gamma-H_\gamma)(47) + \tau(C_\beta-O_\gamma)(35) + \omega(C=O)(9)$	642	647	$\omega(C=O)(52) + \tau(N-C_\alpha)(29)$ (Amide VI)
528	533	$\omega(C=O)(29) + \phi(O=C=N)(19) + \phi(O=C-C_\alpha)(14) + \phi(O_\gamma-C_\beta-C_\alpha)(10)$ (Amide IV + VI)	575	577	$\omega(O_\gamma-H_\gamma)(50) + \tau(C_\beta-O_\gamma)(39)$
369	371	$\phi(N-C_\alpha-C_\beta)(37) + \phi(O_\gamma-C_\beta-C_\alpha)(12) + \omega(C=O)(11) + \nu(C_\alpha-C)(10)$	469	468	$\phi(N-C_\alpha-C)(21) + \phi(O=C-C_\alpha)(15) + \phi(N-C-C_\alpha)(15)$
316	316	$\phi(O=C-C_\alpha)(18) + \phi(C-C_\alpha-C_\beta)(17) + \phi(N-C-C_\alpha)(13) + \omega(C=O)(11) + \phi(O_\gamma-C_\beta-C_\alpha)(10)$	421	430	$\phi(N-C-C_\alpha)(15) + \phi(N-C_\alpha-C_\beta)(13) + \phi(C-C_\alpha-C_\beta)(13)$
261	256	$\phi(O_\gamma-C_\beta-C_\alpha)(27) + \phi(C-C_\alpha-C_\beta)(16) + \tau(N-C_\alpha)(11)$	309	316	$\phi(O_\gamma-C_\beta-C_\alpha)(43) + \phi(O=C=N)(15) + \nu(C_\alpha-C)(12)$
225	233	$\phi(C=N-C_\alpha)(23) + \tau(C_\alpha-C_\beta)(17) + \tau(N-C_\alpha)(13)$	268	268	$\phi(O_\gamma-C_\beta-C_\alpha)(14) + \phi(N-C_\alpha-C)(13) + \phi(C=N-C_\alpha)(13) + \phi(O=C=N)(12) + \tau(C_\alpha-C)(14)$
151	—	$\tau(C_\alpha-C)(33) + \phi(N-C_\alpha-C)(23) + \phi(C-C_\alpha-C_\beta)(9)$	232	233	$\tau(C_\alpha-C)(43) + \tau(C_\alpha-C_\beta)(10)$
142	—	$\tau(C_\alpha-C)(19) + \omega(N-H)(16) + \tau(N-C_\alpha)(15)$	157	—	$\tau(C_\alpha-C_\beta)(39) + \phi(C-C_\alpha-C_\beta)(12) + \omega(C=O)(10) + \tau(C=N)(10)$
120	—	$\tau(C_\alpha-C_\beta)(29) + \phi(C-C_\alpha-C_\beta)(18)$	91	—	$\phi(C-C_\alpha-C_\beta)(30) + \phi(N-C_\alpha-C_\beta)(24) + \tau(C_\alpha-C_\beta)(18)$
81	—	$\tau(C_\alpha-C_\beta)(23) + \phi(N-C_\alpha-C_\beta)(23) + \phi(C=N-C_\alpha)(17)$	67	—	$\tau(N-C_\alpha)(26) + \tau(C=N)(26) + \tau(C_\alpha-C_\beta)(19)$

All frequencies are in cm^{-1}
Only dominant PEDs are given

and Koenig and Sutton[4] (1537 cm^{-1} in i.r. and 1531 cm^{-1} in Raman) for PLS itself and those for other β sheets [1514 cm^{-1} for polyglycine I[20] and 1524 cm^{-1} for β-poly(L-alanine)[21]].

The splitting of the amide I and II bands was found to provide diagnostic criteria for distinguishing between the α helical form, the anti-parallel or parallel chain extended forms and the disordered form[22–24]. For PLS, Koenig and Sutton[4] observed the splittings in the amide I region at 1695 and 1621 cm^{-1} in i.r. and 1668 cm^{-1} in Raman spectra. By using Miyazawa's perturbation calculations[25] they have shown that such splittings in the amide I region is characteristic of an anti-parallel pleated sheet structure. Similar splittings are reported by Bohak and Katchalski[1].

The frequency of the amide III mode does not depend solely on main chain conformation. Side chain structure also plays an important role[26]. The amide III mode calculated at 1251 cm^{-1} at the zone centre is assigned to the peak at 1249 cm^{-1}. On dispersion the contributions

Table 5 Comparison of amide modes of β-PLS with other polypeptides in β form

	PLS		PGI		PLA		PLV	
Amide	$\delta = 0$	$\delta = \pi$	$\delta = 0$	$\delta = \pi$	$\delta = 0$	$\delta = \pi$	$\delta = 0$	$\delta = \pi$
A	3318	3318	3300	3300	3283	3283	3290	3290
I	1637	1628	1690	1630	1695	1634	1638	1638
II	1532	1537	1514	1524	1524	1524	1545	1545
III	1249	1270	1240	1220	1224	1241	1228	1228
IV	533	773	628	773	594	657	548	684
V	713	685	699[a]	700	622	705	715	715
VI	533	647	618[a]	600	594	657	615	628

All frequencies are in cm^{-1}
[a] Marked frequencies are the calculated ones
PLS = poly(L-serine); PGI = polyglycine I; PLA = poly(L-alanine); PLV = poly(L-valine)

from the side chain increase and mix with the amide III. Due to this it is higher than in other β sheets (*Table 5*). At the zone boundary it is calculated at 1275 cm^{-1} and matched to the observed band at 1270 cm^{-1}. These matchings could be made only when the off-diagonal coupling interaction between (N–C_α) and (N=C) was taken into consideration. The motion of these internal coordinates becomes coupled via the motion of the nitrogen atom of the peptide group. Similarly, amide IV mode calculated at 528 cm^{-1} is not a pure mode, but mixed with amide VI mode.

The N–H wagging mode, which gives rise to the amide V band is calculated at 713 cm^{-1} at the zone centre. Its frequency depends on a combination of main-chain conformation, hydrogen-bond strength and side-chain structure. Interchain interactions through hydrogen bonds are not explicitly used in the calculations for the isolated chain, but their effects are indirectly taken into account in the adjustment of force fields.

A peak observed at 1077 cm^{-1}, corresponding to the Raman line at 1082 cm^{-1}, has been assigned to a normal mode at 1083 cm^{-1} involving the C_α–N and C_α–C_β stretch at the $\delta = \pi$ end. The appearance of this band may be of general use in identifying the β sheet conformation[27].

Koenig and Sutton[4] have tentatively assigned the mode at 1304 cm^{-1} due to C_α–H_α bending. Our calculations support this assignment. The dispersion of this mode is small (11 cm^{-1}) with PED showing mainly C_α–H_α bending both at the zone centre as well as at the zone boundary.

Side-chain modes

The side chain of PLS contains one methylene group and a hydroxyl group. The frequency of O–H stretching is observed at 3382 cm^{-1}, which is lower than that in L-serine (at 3500 cm^{-1}). In PLS no absorption in the 3500 cm^{-1} region indicates the presence of hydrogen bonding[1], which lowers the frequency of O–H stretching. The hydrogen bonding is further supported by the fact that PLS is insoluble in water[14] and is yet another pointer towards the possible formation of bifurcated hydrogen bonds.

A strong peak at 1467 cm^{-1} in this region is characteristic of the deformation of a methylene group adjacent to the hydroxyl one[28], and it has been assigned to the scissoring mode. This mode is highly localized and does not disperse.

In the earlier qualitative spectral studies, Koenig and Sutton[4] have assigned a peak observed at 1399 cm^{-1} as due to the O–H in-plane bending mode, whereas Bohak and Ellenbogen[14] assigned this to methylene deformation. Our calculations show that it is mainly an O–H in-plane bending mode (76%) with a small contribution of methylene scissoring (14%). The O–H out-of-plane wagging mode is calculated at 563 cm^{-1} and has been matched to the peak at 564 cm^{-1}, which is the range of the O–H wagging mode in other polymers such as poly(vinyl alcohol)[29]. These assignments could be further confirmed with the help of *O*-deuterated spectra.

Dispersion curves

One of the characteristic features of the dispersion curves is the repulsion and exchange of character between various pairs of modes. Pairs of modes that repel are 718 and 634 cm^{-1}, 563 and 528 cm^{-1} and 151 and 142 cm^{-1}. These occur in the neighbourhood of $\delta = 0.65\pi$, 0.35π and 0.25π, respectively. It is observed that the lower frequency modes of the pairs approach the higher frequency modes and then they diverge after repulsion. Such repulsions occur for modes belonging to the same symmetry species. The dispersion curves of the $\delta = 0$ modes at 1532, 1251 and 81 cm^{-1} have regions of high density-of-states (zero slope regions). Some of the peaks which were unassigned earlier (1556, 1270 and 697 cm^{-1}) get assigned by the frequencies in the high density regions (1546, 1290 and 690 cm^{-1}, respectively). Such regions where $(\partial\omega/\partial k) \rightarrow 0$ are akin to critical points known as Von Hove singularities in lattice dynamics[30]. A knowledge of these is important for obtaining several thermodynamic properties such as specific heat, enthalpy changes, etc. They are more conveniently observable in inelastic incoherent neutron scattering.

In PLS the dispersion curves in the lower frequency region (~100–200 cm^{-1}) come close together at the $\delta = 0$ end, and fan out, appearing to repel each other towards the zone boundary. This feature is also true of the dispersion curves of β-poly(L-alanine)[21], polyethylene[31] and polyglycine I[20], which take the planar zig-zag configuration. This common feature may be due to the absence of strong intrachain interactions stabilizing the structure, in contrast to the case of the hydrogen-bonded α-helix.

An interesting feature in the dispersion curves is the parallelism between the 1342 and 1315 cm^{-1} and 369 and

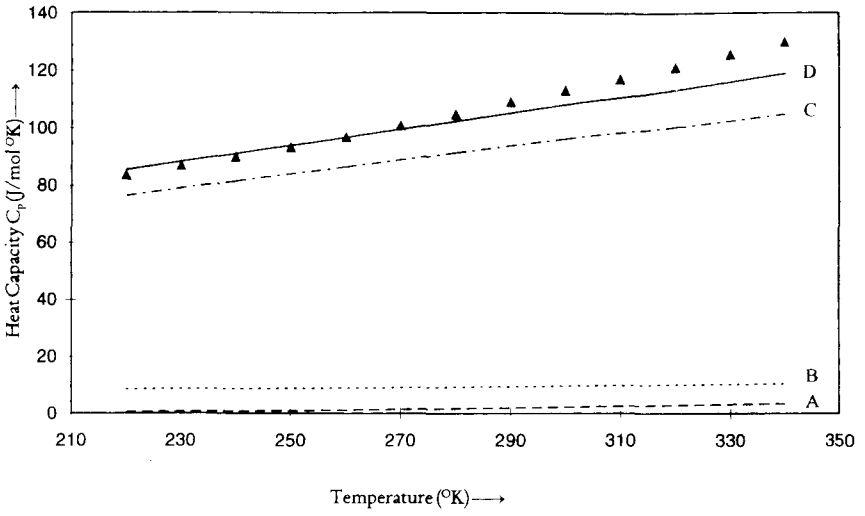

Figure 6 Variation of heat capacity C_p with temperature (the contribution of backbone, side-chain and mixed modes and total heat capacity are shown by curves A, B, C and D, respectively). ▲: Experimental data

316 cm^{-1} pairs of modes. This only indicates that the speed of optical phonons is the same.

The lower frequency modes, especially the acoustic modes, are characteristic of the two-fold helical chain symmetry. The two acoustic branches in the dispersion curves are similar in shape to the dispersion of these branches in other two-fold helical polymers like polyethylene[31], polyglycine[20], syndiotactic polystyrene in its two-fold helical form[32], poly(L-valine)[33], etc. The peaks in the acoustic curves of PLS occur at $\delta = 0.45\pi$ and 0.25π. A comparison with β-PLV shows that, although the peaks in the acoustic curves fall at about the same δ value, the peak heights are different. A profile correlation between helical chain symmetry and the shape of the dispersion curves has been observed earlier for some three-fold polypeptides[34].

Agreement with the experimental values for frequencies at $\delta = 0$ and $\delta = \pi$ shows that basically the profile of the dispersion curves is correct.

Frequency distribution function and specific heat of PLS

The frequency distribution obtained from the dispersion curves for the isolated chain of PLS is plotted in *Figures 3b*, *4b* and *5b*. The peaks in the frequency distribution curves corresponding to the regions of high density-of-states compare well with the observed frequencies. The frequency distribution function is further used in calculating the specific heat of the PLS chain. Experimental heat capacity measurements have been reported by Roles *et al.*[10] for a number of polypeptides. Since the dispersion curves for PLS were not available, for specific heat calculations they used the modes of polyglycine and polyalanine for the backbone information, polyethylene for the vibrational modes of the methyl group and poly(vinyl alcohol) for that of the hydroxyl group. Such transference is not valid unless identical circumstances prevail. As mentioned earlier, separation of vibrational spectra into a group and a skeletal spectrum is valid only in the high frequency region where the backbone and side-chain modes are pure. Below 1200 cm^{-1}, the backbone and side-chain modes become heavily mixed. Modes which are purely skeletal, purely side chain and a mixture of these two are given in *Tables 2*, *3* and *4*, respectively. Their contributions to the heat capacity are shown in *Figures 6a*, *6b* and *6c*, respectively, in the temperature range 200–380 K. The total heat capacity is shown in *Figure 6* by a continuous line, and ▲ represents the experimental data of Roles *et al.*[10]. It is clear from *Figure 6* that the major contribution to the specific heat comes from backbone and side-chain coupled modes. The calculations are in good agreement in the low temperature region. Above 280 K the experimental values are consistently higher than the calculated ones because of the onset of the glass transition. An X-ray diffraction pattern of the sample also confirms this, revealing a low degree of crystallinity (about 15%)[10]. At the glass transition temperature (T_g) the amorphous state of the polypeptide passes into a metastable thermodynamic state—the so-called glassy state, having greater free energy than that of the crystalline state and above T_g the molecules have all the mobility characteristics of a liquid. Hence, the specific heat will be considerably affected because of the additional complex segmental motions. Present theoretical calculations do not take these motions into account.

Although the calculated specific heat is in good agreement, with the experimental one below 280 K, the contribution from the lattice modes is bound to make a difference to the specific heat at low temperature. At the moment the calculation of dispersion curves for a three-dimensional crystal is extremely difficult because of the large matrix size and enormous number of interactions.

ACKNOWLEDGEMENTS

Financial assistance to A.G. and V.D.G. (under the Emeritus Scientist Scheme) from the Council for Scientific and Industrial Research is gratefully acknowledged. The authors are also grateful to Dr V. P. Gupta for providing the sample and to Sri S. M. Gupta of the RSIC at the Central Drug Research Institute, Lucknow, for providing facilities to use the *FT* i.r. spectrophotometer.

REFERENCES

1. Bohak, Z. and Katchalski, E., *Biochemistry*, 1963, **2**, 228.
2. Fasman, G. D. and Blout, E. R., *J. Am. Chem. Soc.*, 1960, **82**, 2262.

3. Blout, E. R., Loze, C. de, Bloom, S. M. and Fasman, G. D., *J. Am. Chem. Soc.*, 1960, **82**, 3787.
4. Koenig, J. L. and Sutton, P. L., *Biopolymers*, 1971, **10**, 89.
5. Sarathy, K. P. and Ramchandran, G. N., *Biopolymers*, 1968, **6**, 461.
6. Chou, K. C., Nemethy, G. and Scheraga, H. A., *Biochemistry*, 1983, **22**, 6213.
7. Wunderlich, B. and Bu, H. S., *Thermochimica Acta*, 1987, **119**, 225.
8. Bu, H. S., Aycock, W., Cheng, S. Z. D. and Wunderlich, B., *Polymer*, 1988, **29**, 1486.
9. Roles, K. A. and Wunderlich, B., *Biopolymers*, 1991, **31**, 477.
10. Roles, K. A., Xenopoulos, A. and Wunderlich, B., *Biopolymers*, 1993, **33**, 753.
11. Singh, R. D. and Gupta, V. D., *Spectrochimica Acta*, 1971, **27A**, 385.
12. Fanconi, B., Small, E. W. and Peticolas, W. L., *Biopolymers*, 1971, **10**, 1277.
13. Krishnan, M. V. and Gupta, V. D., *Chem. Phys. Lett.*, 1970, **7**, 285.
14. Bohak, Z. and Ellenbogen, E., *Bull. Res. Council Israel*, 1960, **9A**, 119.
15. Wilson, E. B., Jr, *J. Chem. Phys.*, 1939, **7**, 1047.
16. Wilson, E. B., Jr, *J. Chem. Phys.*, 1941, **9**, 76.
17. Wilson, E. B., Jr, Decius, J. C. and Cross, P. C., *Molecular Vibrations: The Theory of Infrared and Raman Vibrational Spectra*. Dover Publications, New York, 1980.
18. Higgs, P. W., *Proc. Roy. Soc. (London)*, 1953, **A220**, 472.
19. Pan, R., Verma, M.-N. and Wunderlich, B., *J. Therm. Anal.*, 1989, **35**, 955.
20. Gupta, V. D., Trevino, S. and Boutin, H., *J. Chem. Phys.*, 1968, **48**, 3008.
21. Krishnan, M. V. and Gupta, V. D., *Indian J. Pure and Appl. Phys.*, 1972, **10**, 210.
22. Ambrose, E. J. and Elliott, A., *Proc. Roy. Soc. (London)*, 1951, **A205**, 47.
23. Elliott, A., *Proc. Roy. Soc. (London)*, 1953, **A221**, 104.
24. Miyazawa, T. and Blout, E. R., *J. Am. Chem. Soc.*, 1961, **83**, 712.
25. Miyazawa, T., *J. Chem. Phys.*, 1960, **32**, 1647.
26. Krimm, S. and Bandekar, J., *Adv. Protein Chem.*, 1986, **38**, 181.
27. Frushour, B. G. and Koenig, J. L., *Biopolymers*, 1974, **13**, 455.
28. Colthup, N. B., Wiberly, S. E. and Daly, L. H., *Introduction to Infrared and Raman Spectroscopy*. Academic Press, New York, 1964, p. 225.
29. Zbindin, R., *Infrared Spectroscopy of High Polymers*. Academic Press, New York and London, 1969, p. 96.
30. Callaway, J., *Quantum Theory of Solids*. Academic Press, New York and London, 1974, pp. 30–35.
31. Tasumi, M. and Shimanouchi, T., *J. Molecular Spectroscopy*, 1962, **9**, 261.
32. Rastogi, S. and Gupta, V. D., *J. Macromol. Sci.—Phys. B*, 1995, **34**, 1.
33. Burman, L., Tandon, P., Gupta, V. D. and Srivastava, S., *Polymer J.*, 1995, **27**, 481.
34. Gupta, V. D., *Int. J. Quantum Chem.*, 1981, **20**, 9.